

Localization properties in Lieb lattices and their extensions

Jie Liu^a, Xiaoyu Mao^a, Jianxin Zhong^a, Rudolf A. Römer^{a,b}

^a*School of Physics and Optoelectronics, Xiangtan University, Xiangtan 411105, China*

^b*Department of Physics, University of Warwick, Coventry, CV4 7AL, United Kingdom*

Abstract

We study the localization properties of generalized, two- and three-dimensional Lieb lattices, $\mathcal{L}_2(n)$ and $\mathcal{L}_3(n)$, $n = 1, 2, 3$ and 4, at energies corresponding to flat and dispersive bands using the transfer matrix method (TMM) and finite size scaling (FSS). We find that the scaling properties of the flat bands are different from scaling in dispersive bands for all $\mathcal{L}_d(n)$. For the $d = 3$ dimensional case, states are extended for disorders W down to $W = 0.01t$ at the flat bands, indicating that the disorder can lift the degeneracy of the flat bands quickly. The phase diagram with periodic boundary condition for $\mathcal{L}_3(1)$ looks similar to the one for hard boundaries [1]. We present the critical disorder W_c at energy $E = 0$ and find a decreasing W_c for increasing n for $\mathcal{L}_3(n)$, up to $n = 3$. Last, we show a table of FSS parameters including so-called irrelevant variables; but the results indicate that the accuracy is too low to determine these reliably.

Keywords: Localization, Flat band, Phase diagram, Finite size scaling

1. Introduction

Flat band systems, in which the absence of a dispersion in the band structure leads to a highly dramatic macroscopic degeneracy, have at the flat band energy an effectively reduced kinetic energy. Hence other terms in the Hamiltonian can become prominent, such as many-body interactions. This mechanism leads to a convenient construction of various platform for studying many-body physics, such as the fractional quantum Hall effect [2, 3, 4], spin liquids [5, 6], ferromagnetism [7, 8], and superconductivity [9, 10, 11]. In recent years, artificial lattices [12], for instance, in photonic [13, 14, 15, 16, 17, 18] and cold atom systems [19, 20, 21], allow to realize experimentally also the probing of the *novel* many-body problems.

As is well known, states in a flat band are localized [14] because of the high degeneracy. Hence disorder, which one should expect to destroy this degeneracy, might also, at least initially, destroy the localization. So what will happen after disorder is being included in the Hamiltonians describing these localized flat bands is an interesting question.

Flat band system can be constructed in many models [2, 3, 4, 8, 22]. The Lieb lattice [10, 23, 24] is one of the simplest and most famous two-dimensional flat band system. Actually, the CuO_2 plane of cuprate superconductors is also a Lieb lattice, namely $\mathcal{L}_2(1)$ in our notation. It contains three atoms per unit cell as shown in Fig. 1(a). In the figure, we also introduce its

Email addresses: liujie@smail.xtu.edu.cn (Jie Liu), Maoxiaoyu@smail.xtu.edu.cn (Xiaoyu Mao), jxzhong@xtu.edu.cn (Jianxin Zhong), r.roemer@warwick.ac.uk (Rudolf A. Römer)

Preprint submitted to Annals of Physics Special Issue: Localisation 2020

August 3, 2021

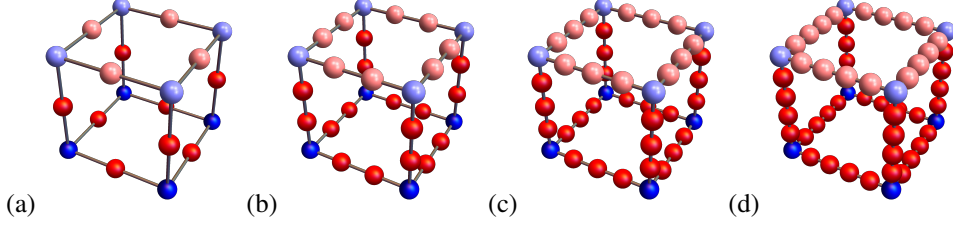


Figure 1: Schematic representation of Lieb and extended Lieb lattices $\mathcal{L}_d(n)$. The lightly coloured spheres highlight the situation in 2D while together with the fully coloured spheres they represent the 3D lattices. Blue spheres denote undecimated lattices site while the red sphere will be decimated in the TMM formulation. The dark lines are guides to the eye only. The labels (a), (b), (c) and (d) denote $\mathcal{L}_2(1)/\mathcal{L}_3(1)$, $\mathcal{L}_2(2)/\mathcal{L}_3(2)$, $\mathcal{L}_2(3)/\mathcal{L}_3(3)$ and $\mathcal{L}_2(4)/\mathcal{L}_3(4)$, respectively.

extensions $\mathcal{L}_2(n)$, $n = 2, 3$ and 4 , shown in panels (b)-(d), respectively. The three-dimensional Lieb lattice and its extensions are also shown in Fig. 1(a)-(d). The number of flat bands is related to the number of central red atoms between two nearest blue atoms. In short, for $\mathcal{L}_d(n)$, the number of flat band is n with $d - 1$ degeneracy. The central energy at $E = 0$ is part of a flat band for $\mathcal{L}_2(1)$, $\mathcal{L}_2(3)$, $\mathcal{L}_3(1)$ and $\mathcal{L}_3(3)$ while it remains in a dispersive band for $\mathcal{L}_2(2)$, $\mathcal{L}_2(4)$, $\mathcal{L}_3(2)$ and $\mathcal{L}_3(4)$ [25, 1].

This paper is organized as follows. In section 2 and section 3 we will discuss the two-dimensional and three-dimensional Lieb lattices and their extensions, respectively. The conclusion is given in section 4.

2. The two-dimensional Lieb lattice and its extensions

2.1. Previous results for disordered $\mathcal{L}_2(n)$ lattices

In our previous paper [25], we study the localization properties of $\mathcal{L}_2(n)$ in detail. Using direct diagonalization for small system sizes, we compute the density of states (DOS). We can see that in the presence of disorder, the interplay between flat bands and dispersive bands is prominent for all $\mathcal{L}_2(n)$, $n = 1, 2, 3$ and 4 . The disorder can quickly lift the degeneracy of flat bands and make the states merge with the neighboring dispersive bands. When $W \gtrsim 2$, the flat band DOS loses its peaks distinguishing and becomes part of a large bulk DOS.

Next, we use a renormalized transfer-matrix method (TMM) and compute the reduced localization lengths $\Lambda_M(E, W) = \lambda(E, W)/M$, where M corresponds to the width of the quasi-1D transfer-matrix strip. For all $\mathcal{L}_d(n)$, we find that for $W \gtrsim t$ all states are localized. The localization lengths for states at flat band energies are about one order of magnitude smaller than for states from dispersive bands. We employ traditional one-parameter finite-size scaling methods to estimate a scaling parameter $\xi(E, W)$ [26]. The $\Lambda(E, W)/M$ can be described after scaling by a single scaling branch, corresponding to a fully localized behaviour. After fitting the ξ with disorder W , we use three fitting forms, power law form as $\xi(W) \propto W^{-2}$ [27], a non-universal form $\xi(W) = aW^{-\alpha} \exp(\beta W^{-\gamma})$ and a constraint form $\xi(W) = aW^{-2} \exp(\beta W^{-1})$. For $\mathcal{L}_2(1)$ and $\mathcal{L}_2(3)$ at the flat band energy $E = 0$, we find that the usual power law form $\xi(W) \propto W^{-2}$ for 1D localization fits well for disorder around $1 < W < 2$. However, for $\mathcal{L}_2(2)$ and $\mathcal{L}_2(4)$ at $E = 0$, which is an energy in a dispersive band for these lattices, none of the fits gives a convincing result.

2.2. Scaling function Λ_M vs reduced correlation length ξ_M for $\mathcal{L}_2(n)$

The scaled localization lengths $\Lambda_M(0, W)$ as a function of scaled correlation length ξ/M for $\mathcal{L}_2(n)$, $n = 1, 2, 3$ and 4 are shown in Fig. 2(a) at energy $E = 0$. This corresponds to flat bands for $\mathcal{L}_2(1)$ and $\mathcal{L}_2(3)$ and dispersive band for $\mathcal{L}_2(2)$ and $\mathcal{L}_2(4)$. The $\Lambda_M(0, W)$ data all show the behaviour for localized states, scaling as $\Lambda_M(0, W) \propto \xi(0, W)/M$ for large system sizes and large disorders. In this regime, the behaviour of states in the flat bands and in the dispersive bands is similar as shown also in the inset graph of said figure.

2.3. Scaling parameter ξ vs disorder W for $\mathcal{L}_2(n)$

The disorder dependence of the scaling parameter ξ for small disorders $t \leq W \leq 2t$ is shown in Fig. 2(b), computed from the $\Lambda_M(E = 0, W)$ data of Fig. 2(a). We see that the behaviour of ξ for $\mathcal{L}_2(1)$ is comparable to $\mathcal{L}_2(3)$; both are well-described by a power law ax^b with exponent approximately $b \sim -2$, similar to localization properties of a standard 1D Anderson model [27]. This might suggest that the localization behaviour of these flat band states at least for weak disorder is similar to the 1D behaviour. On the other hand, for the dispersive states of $\mathcal{L}_2(2)$ and $\mathcal{L}_2(4)$ at $E = 0$, we find that the values of ξ are orders of magnitude larger than for $\mathcal{L}_2(1)$ and $\mathcal{L}_2(3)$. The simple power-law also does not fit anymore and we rather see the more standard behaviour of a 2D Anderson model [27] with a quickly diverging ξ when $W \rightarrow 0$. Nevertheless, for both flat band and dispersive band energies, the fits are not very robust and have rather small p values of $< 10^{-10}$. This shows that the true form of the behaviour of $\xi(W \rightarrow 0)$ is yet to be determined.

2.4. Density of states without Gaussian broadening for $\mathcal{L}_2(n)$

The results of the disorder-averaged density of states (DOS), calculated with direct diagonalization, are shown in Fig. 3. The system sizes are $M^2 = 13^2, 10^2, 9^2, 8^2$ for $\mathcal{L}_2(n)$, $n = 1, 2, 3$ and 4 , respectively. The disorder ranges from $W = 0$ to $W = 5.2$ in step of 0.05 using 300 independent random samples. We can see the prominent peaks of flat bands close to $W = 0$ have been largely vanished when the disorder reaches up to $W = 2$ for all $\mathcal{L}_2(n)$, $n = 1, 2, 3$ and 4 .

3. Three-dimensional Lieb lattice and its extensions

3.1. Previous results for disordered $\mathcal{L}_3(n)$ lattices

In Ref. [1], we investigated the DOS, the localization properties and the phase diagrams for the 3D Lieb lattices $\mathcal{L}_3(n)$, $n = 1, 2, 3$ and 4 as shown in Fig. 1. Obviously, the main difference to the 2D case is the existence of an Anderson metal insulator transition (MIT) in 3D Lieb lattices [1]. Details of the TMM construction for $\mathcal{L}_3(n)$ can also be found in Ref. [1] along with finite-size scaling results for the universal critical exponent ν of the localization lengths. We found ν to be in good agreement with the currently accepted value of $\nu = 1.590(1.579, 1.602)$ [28, 29] for the Anderson transition. In the following, we shall elaborate on the stability of the phase diagrams to a change in boundary conditions, highlight the various positions of the transitions in the phase diagrams, comment on the possibility of FSS with irrelevant scaling parameters and also provide the DOS without Gaussian-broadening.

3.2. Phase diagram with periodic boundary condition for $\mathcal{L}_3(1)$

The phase diagrams given in Ref. [1] have been computed for the $\mathcal{L}_3(n)$ lattices with hard wall boundaries. In Fig. 4(a) we now show a phase diagram for $\mathcal{L}_3(1)$ with periodic boundary condition. The phases have been determined by the scaling behaviour of the $\Lambda_M(E, W)$ for system sizes $M = 4$, $M = 6$ and $M = 8$ with error $\leq 0.1\%$ [30]. Comparing this to the results obtained with hard boundary conditions, we find that it looks very similar as expected although the extended region is a little wider in the E axis. As for the hard wall case, we can identify a re-entrant region around disorder $W = 4$ and a shoulder at $E \sim 3$ and $W \sim 6$. Hence as expected, the change in boundary conditions does not change the phase diagrams appreciably already with the small system sizes and modest disorder averages as used here and in Ref. [1].

3.3. Localization and extended transition with $0.01 \leq W \leq 2.0$

For $W < 1$, it is well known that the convergence of the TMM is very slow. Hence results for appropriately small errors are hard to compute. Usually, this is not a problem since, e.g., in the 3D Anderson model, the limit as $W \rightarrow 0$ belongs trivially to the extended phase. However, for the $\mathcal{L}_3(n)$ lattice, we know that at the flat band energies even at $W = 0$, we expect compactly localized states [31, 32]. Hence it is interesting to see if the localization properties at $W < 1$ for flat band energies indicate any possible “inverse” Anderson transition from extended states at $W \sim 1$ to localized states at small, but finite $W > 0$.

In Ref. [1], we had shown that at the flat band energy $E = 0$ for $\mathcal{L}_3(1)$ and at $E = 1$ for $\mathcal{L}_3(2)$, the Λ_M increases with increasing M , indicating extended behaviour, down to disorders as small as $W = 0.01$. In Fig. 5(a-c), we now augment that result by studying energies close by. For $\mathcal{L}_3(1)$ and $E = 0.05$ we initially find localized behaviour, e.g., Λ_M decreasing with increasing M up to $M = 10$, but then reversing to extended behaviour for larger M . For $E = 0.1$ the reversal to the extended behaviour already starts at $M = 8$ while for $E = 0.15$, only the extended behaviour remains. In Fig. 5(d), we see that for $\mathcal{L}_3(1)$ at $E = 1.05$, the Λ_M decreases with increasing M . This localized behaviour should vanish for larger M values, but it is at present beyond our computational capabilities.

We conclude that the presence of the compactly localized states at the flat band energies certainly has an effect at small disorder, but for larger disorder values, the broadening of the flat bands and the mixing with the dispersive bands becomes dominant such that the character of the states is extended down to disorders $W = 0.01$. This is usually already true at $W \sim 0.1$.

3.4. Divergence of the scaling parameter $\xi(W)$

The behaviour of $\xi(W)$ for $\mathcal{L}_3(1)$, $\mathcal{L}_3(2)$ and $\mathcal{L}_3(3)$ is given in Fig. 4. We can clearly see how the critical disorder W_c decreases from 8.59 for $\mathcal{L}_3(1)$ to 5.96 for $\mathcal{L}_3(2)$ and finally to 4.79 for $\mathcal{L}_3(3)$. This suggests that a larger n in $\mathcal{L}_3(n)$, i.e. a larger number of additional (red, cp. Fig. 1) atoms, leads to stronger localization and hence an MIT already for smaller values of W_c . It could be an interesting study to estimate $W_c(n)$, particularly the limiting behaviour when $n \rightarrow \infty$.

3.5. Scaling with irrelevant variables n_i, m_i

For high-precision estimates of critical properties, including ν , it is by now state of the art to include irrelevant scaling contributions, i.e. scaling as M^{-y} with $y > 0$, in the FSS analysis. However, such FSS methods also require large M values to reliably model the irrelevant scaling. Due to the complexity of the $\mathcal{L}_3(n)$ systems, only values of $M \leq 20$ have been computed in Ref. [1]. For such sizes, adding irrelevant scaling variables is usually not a net benefit. In Table 1, we

show the results for FSS with and without scaling. We note that although acceptable p values can be obtained for the fits with irrelevant scaling exponent y included, in nearly all cases, this results either in increased error estimates for the relevant exponent ν . Alternatively, one finds estimates for y with very large errors or very large values for y . Except for one case, the final estimate for the physical quantity ν has hardly changed. Hence we conclude that for the available Λ_M data, the inclusion of irrelevant scaling parameter y does not necessarily add towards the accuracy of the estimates for ν . This confirms having made this choice in Ref. [1].

$\mathcal{L}_3(1)$										
ΔM	E	δW	n_r, n_i, m_r, m_i	W_c	$CI(W_c)$	ν	$CI(\nu)$	y	$CI(y)$	p
16-20	0	8.25-8.9	3 0 1 0	8.59 (58, 61)	1.6	(4, 7)	0	0	0.15	
16-20	0	8.25-8.9	2 1 1 1	8.71(57, 84)	1.3	(0.8, 1.8)	4	(-2, 10)	0.86	
14-20	1	8.0-8.8	3 0 1 0	8.44 (42, 45)	1.6	(5, 7)	0	0	0.18	
14-20	1	8.0-8.8	3 2 1 1	8.48(45, 50)	1.8	(6, 9)	6.9	(6.6, 7.1)	0.77	
ΔM	W	δE	n_r, n_i, m_r, m_i	E_c	$CI(E_c)$	ν	$CI(\nu)$	y	$CI(y)$	p
16-20	3	3.725-3.785	2 0 1 0	3.75 (74, 75)	1.7	(6, 9)	0	0	0.88	
16-20	3	3.725-3.785	3 2 1 2	3.75(74, 75)	1.5	(0.6, 2.5)	2	(-3, 8)	0.7	
16-20	6	3.04-3.11	1 0 1 0	3.08 (07, 09)	1.5	(1.0, 2.1)	0	0	0.14	
16-20	6	3.04-3.11	1 1 2 1	3.08(06, 09)	1.5	(0.7, 2.4)	47	(44, 50)	0.13	
$\mathcal{L}_3(2)$										
ΔM	E	δW	n_r, n_i, m_r, m_i	W_c	$CI(W_c)$	ν	$CI(\nu)$	y	$CI(y)$	p
12,14,18	0	5.85-6.05	2 0 2 0	5.96 (95, 97)	1.8	(1.5, 2.0)	0	0	0.08	
12,14,18	0	5.85-6.05	2 1 1 4	5.97(96, 98)	1.7	(1.3, 2.1)	9	(2, 16)	0.89	
ΔM	W	δE	n_r, n_i, m_r, m_i	E_c	$CI(E_c)$	ν	$CI(\nu)$	y	$CI(y)$	p
10-14	4	1.6-1.8	2 0 1 0	1.70 (70, 71)	1.6	(4, 7)	0	0	0.18	
10-14	4	1.6-1.8	1 1 2 1	1.72(67, 78)	1.6	(1.1, 2.1)	6	(-18, 31)	0.38	
$\mathcal{L}_3(3)$										
ΔM	E	δW	n_r, n_i, m_r, m_i	W_c	$CI(W_c)$	ν	$CI(\nu)$	y	$CI(y)$	p
12-18	0	4.7-4.875	2 0 1 0	4.79 (78, 80)	1.6	(4, 8)	0	0	0.43	
12-18	0	4.7-4.875	2 1 1 2	4.79(78, 80)	1.6	(4, 8)	8284	(0, 1)	0.11	

Table 1: Critical parameters at the MIT for $\mathcal{L}_3(n)$, $n = 1, 2$ and 3 . The columns are denoting the system width M , fixed E (or W), the range of W (or E). The expansion orders n_r, n_i, m_r, m_i are listed as well as the obtained critical disorders W_c (or energies E_c), their 95% confidence intervals (CI), the critical exponent ν , its CI, the irrelevant parameter y , its CI, and the goodness of fit probability p . The confidence interval are given with one significant decimal. For instance, 1.6(4, 8) marks that the CI is (1.4, 1.8)

3.6. Density of states without Gaussian broadening for $\mathcal{L}_3(n)$

The results of for the DOS, calculated with exact diagonalization and without applied Gaussian smoothing, are in Fig. 3. The system sizes are $M^3 = 5^3, 5^3, 4^3, 4^3$ for $\mathcal{L}_3(n)$, $n = 1, 2, 3$ and

4, respectively. The disorder ranges are all from $W = 0$ to $W = 5.2$ in step of 0.05 and with 300 samples for $n = 1, 2, 3$ but only 100 samples for $\mathcal{L}_3(4)$ because of computing time limits. Again, the results are very similar to the Gaussian-broadened DOS shown in Ref. [1].

4. Conclusions

We have studied the localization properties of the 2D and 3D extended Lieb lattices. Clearly, the Lieb lattices exhibit stronger localization than their more standard square and cubic Anderson lattices. This can be understood by noting that the transport along the "extra" sites as shown (by red spheres) in Fig. 1 is essentially one-dimensional and hence subject to stronger localization. Consequently, in 2D rather small W values can still be studied (most earlier TMM studies for the 2D Anderson model stop already around $W \sim 2$, cp. Fig. (3) of Ref. [33]). Details of the resulting FSS curves for small W are given in Fig. 2. In 3D, we similarly see that $W_c(n)$ decreases as a function of n . Results for particularly small W are shown in Fig. 5. Due to the numerical complexity of the $\mathcal{L}_d(n)$ systems, scaling is more challenging than in the Anderson models and only relatively small M values can be reached. Table 1 shows that for the available data, there is no need to include irrelevant scaling variables — within the accuracy of the calculation, all estimates of the critical exponent agree with the value found for the Anderson universality class [28, 29].

References

- [1] J. Liu, X. Mao, J. Zhong, R. A. Römer, Localization, phases, and transitions in three-dimensional extended Lieb lattices, *Physical Review B* 102 (17) (2020) 174207. doi:10.1103/PhysRevB.102.174207.
URL <https://link.aps.org/doi/10.1103/PhysRevB.102.174207>
- [2] E. Tang, J.-W. Mei, X.-G. Wen, High-Temperature Fractional Quantum Hall States, *Physical Review Letters* 106 (23) (2011) 236802. doi:10.1103/PhysRevLett.106.236802.
URL <https://link.aps.org/doi/10.1103/PhysRevLett.106.236802>
- [3] T. Neupert, L. Santos, C. Chamon, C. Mudry, Fractional Quantum Hall States at Zero Magnetic Field, *Physical Review Letters* 106 (23) (2011) 236804. doi:10.1103/PhysRevLett.106.236804.
URL <https://link.aps.org/doi/10.1103/PhysRevLett.106.236804>
- [4] K. Sun, Z. Gu, H. Katsura, S. Das Sarma, Nearly Flatbands with Nontrivial Topology, *Physical Review Letters* 106 (23) (2011) 236803. doi:10.1103/PhysRevLett.106.236803.
URL <https://link.aps.org/doi/10.1103/PhysRevLett.106.236803>
- [5] L. Savary, L. Balents, Quantum spin liquids: a review, *Reports on Progress in Physics* 80 (1) (2017) 016502. doi:10.1088/0034-4885/80/1/016502.
URL <https://iopscience.iop.org/article/10.1088/0034-4885/80/1/016502>
- [6] L. Balents, Spin liquids in frustrated magnets, *Nature* 464 (7286) (2010) 199–208. doi:10.1038/nature08917.
URL <http://www.nature.com/articles/nature08917>
- [7] A. Mielke, H. Tasaki, Ferromagnetism in the Hubbard model, *Communications in Mathematical Physics* 158 (2) (1993) 341–371. doi:10.1007/BF02108079.
URL <http://link.springer.com/10.1007/BF02108079>
- [8] H. Tasaki, From Nagaoka's Ferromagnetism to Flat-Band Ferromagnetism and Beyond: An Introduction to Ferromagnetism in the Hubbard Model, *Progress of Theoretical Physics* 99 (4) (1998) 489–548. doi:10.1143/PTP.99.489.
URL <https://academic.oup.com/ptp/article-lookup/doi/10.1143/PTP.99.489>
- [9] S. Miyahara, S. Kusuta, N. Furukawa, BCS theory on a flat band lattice, *Physica C: Superconductivity* 460-462 (2007) 1145–1146. doi:10.1016/j.physc.2007.03.393.
URL <https://linkinghub.elsevier.com/retrieve/pii/S0921453407004261>
- [10] A. Julku, S. Peotta, T. I. Vanhala, D. H. Kim, P. Törmä, Geometric Origin of Superfluidity in the Lieb-Lattice Flat Band, *Physical Review Letters* 117 (4) (2016) 045303. doi:10.1103/PhysRevLett.117.045303.
URL <https://link.aps.org/doi/10.1103/PhysRevLett.117.045303>

- [11] N. B. Kopnin, T. T. Heikkilä, G. E. Volovik, High-temperature surface superconductivity in topological flat-band systems, *Physical Review B* 83 (22) (2011) 220503. doi:10.1103/PhysRevB.83.220503.
URL <https://link.aps.org/doi/10.1103/PhysRevB.83.220503>
- [12] D. Leykam, A. Andreanov, S. Flach, Artificial flat band systems: from lattice models to experiments, *Advances in Physics: X* 3 (1) (2018) 1473052. doi:10.1080/23746149.2018.1473052.
URL <https://www.tandfonline.com/doi/full/10.1080/23746149.2018.1473052>
- [13] S. Mukherjee, A. Spracklen, D. Choudhury, N. Goldman, P. Öhberg, E. Andersson, R. R. Thomson, Observation of a Localized Flat-Band State in a Photonic Lieb Lattice, *Physical Review Letters* 114 (24) (2015) 245504. doi:10.1103/PhysRevLett.114.245504.
URL <https://link.aps.org/doi/10.1103/PhysRevLett.114.245504>
- [14] R. A. Vicencio, C. Cantillano, L. Morales-Inostroza, B. Real, C. Mejía-Cortés, S. Weimann, A. Szameit, M. I. Molina, Observation of Localized States in Lieb Photonic Lattices, *Physical Review Letters* 114 (24) (2015) 245503. doi:10.1103/PhysRevLett.114.245503.
URL <https://link.aps.org/doi/10.1103/PhysRevLett.114.245503>
- [15] D. Guzmán-Silva, C. Mejía-Cortés, M. A. Bandres, M. C. Rechtsman, S. Weimann, S. Nolte, M. Segev, A. Szameit, R. A. Vicencio, Experimental observation of bulk and edge transport in photonic Lieb lattices, *New Journal of Physics* 16 (6) (2014) 063061. doi:10.1088/1367-2630/16/6/063061.
URL <https://iopscience.iop.org/article/10.1088/1367-2630/16/6/063061>
- [16] F. Diebel, D. Leykam, S. Kroesen, C. Denz, A. S. Desyatnikov, Conical Diffraction and Composite Lieb Bosons in Photonic Lattices, *Physical Review Letters* 116 (18) (2016) 183902. doi:10.1103/PhysRevLett.116.183902.
URL <https://link.aps.org/doi/10.1103/PhysRevLett.116.183902>
- [17] S. Taie, H. Ozawa, T. Ichinose, T. Nishio, S. Nakajima, Y. Takahashi, Coherent driving and freezing of bosonic matter wave in an optical Lieb lattice, *Science Advances* 1 (10) (2015) e1500854. doi:10.1126/sciadv.1500854.
URL <https://advances.sciencemag.org/lookup/doi/10.1126/sciadv.1500854>
- [18] M. Nixon, E. Ronen, A. A. Friesem, N. Davidson, Observing Geometric Frustration with Thousands of Coupled Lasers, *Physical Review Letters* 110 (18) (2013) 184102. doi:10.1103/PhysRevLett.110.184102.
URL <https://link.aps.org/doi/10.1103/PhysRevLett.110.184102>
- [19] R. Shen, L. B. Shao, B. Wang, D. Y. Xing, Single Dirac cone with a flat band touching on line-centered-square optical lattices, *Physical Review B* 81 (4) (2010) 041410. doi:10.1103/PhysRevB.81.041410.
URL <https://link.aps.org/doi/10.1103/PhysRevB.81.041410>
- [20] N. Goldman, D. F. Urban, D. Bercioux, Topological phases for fermionic cold atoms on the Lieb lattice, *Physical Review A* 83 (6) (2011) 063601. doi:10.1103/PhysRevA.83.063601.
URL <https://link.aps.org/doi/10.1103/PhysRevA.83.063601>
- [21] V. Apaja, M. Hyrkäs, M. Manninen, Flat bands, Dirac cones, and atom dynamics in an optical lattice, *Physical Review A* 82 (4) (2010) 041402. doi:10.1103/PhysRevA.82.041402.
URL <https://link.aps.org/doi/10.1103/PhysRevA.82.041402>
- [22] C. Weeks, M. Franz, Topological insulators on the Lieb and perovskite lattices, *Physical Review B* 82 (8) (2010) 085310. doi:10.1103/PhysRevB.82.085310.
URL <https://link.aps.org/doi/10.1103/PhysRevB.82.085310>
- [23] E. H. Lieb, Two theorems on the Hubbard model, *Physical Review Letters* 62 (10) (1989) 1201–1204. doi:10.1103/PhysRevLett.62.1201.
URL <https://link.aps.org/doi/10.1103/PhysRevLett.62.1201>
- [24] W.-X. Qiu, S. Li, J.-H. Gao, Y. Zhou, F.-C. Zhang, Designing an artificial Lieb lattice on a metal surface, *Physical Review B* 94 (24) (2016) 241409. doi:10.1103/PhysRevB.94.241409.
URL <https://link.aps.org/doi/10.1103/PhysRevB.94.241409>
- [25] X. Mao, J. Liu, J. Zhong, R. A. Römer, Disorder effects in the two-dimensional Lieb lattice and its extensions, *Physica E: Low-Dimensional Systems and Nanostructures* 124 (January) (2020) 114340. doi:10.1016/j.physe.2020.114340.
URL <https://doi.org/10.1016/j.physe.2020.114340>
- [26] A. MacKinnon, B. Kramer, One-Parameter Scaling of Localization Length and Conductance in Disordered Systems, *Physical Review Letters* 47 (21) (1981) 1546–1549. doi:10.1103/PhysRevLett.47.1546.
URL <https://link.aps.org/doi/10.1103/PhysRevLett.47.1546>
- [27] A. MacKinnon, B. Kramer, The scaling theory of electrons in disordered solids: Additional numerical results, *Zeitschrift für Physik B Condensed Matter* 53 (1) (1983) 1–13. doi:10.1007/BF01578242.
URL <http://link.springer.com/10.1007/BF01578242>
- [28] K. Slevin, T. Ohtsuki, Corrections to Scaling at the Anderson Transition, *Physical Review Letters* 82 (2) (1999) 382–385. doi:10.1103/PhysRevLett.82.382.
URL <https://link.aps.org/doi/10.1103/PhysRevLett.82.382>
- [29] A. Rodriguez, L. J. Vazquez, K. Slevin, R. A. Römer, Multifractal finite-size scaling and universality at the Ander-

- son transition, *Physical Review B* 84 (13) (2011) 134209. doi:10.1103/PhysRevB.84.134209.
URL <https://link.aps.org/doi/10.1103/PhysRevB.84.134209>
- [30] A. Eilmes, A. M. Fischer, R. A. Römer, Critical parameters for the disorder-induced metal-insulator transition in fcc and bcc lattices, *Physical Review B* 77 (24) (2008) 245117. doi:10.1103/PhysRevB.77.245117.
URL <https://link.aps.org/doi/10.1103/PhysRevB.77.245117>
- [31] H. Aoki, M. Ando, H. Matsumura, Hofstadter butterflies for flat bands, *Physical Review B* 54 (24) (1996) R17296–R17299. doi:10.1103/PhysRevB.54.R17296.
URL <https://link.aps.org/doi/10.1103/PhysRevB.54.R17296>
- [32] W. Maimaiti, A. Andreanov, H. C. Park, O. Gendelman, S. Flach, Compact localized states and flat-band generators in one dimension, *Physical Review B* 95 (11) (2017) 115135. doi:10.1103/PhysRevB.95.115135.
URL <https://link.aps.org/doi/10.1103/PhysRevB.95.115135>
- [33] M. Leadbeater, R. Römer, M. Schreiber, Interaction-dependent enhancement of the localisation length for two interacting particles in a one-dimensional random potential, *The European Physical Journal B* 8 (4) (1999) 643–652. doi:10.1007/s100510050732.
URL <http://link.springer.com/10.1007/s100510050732>

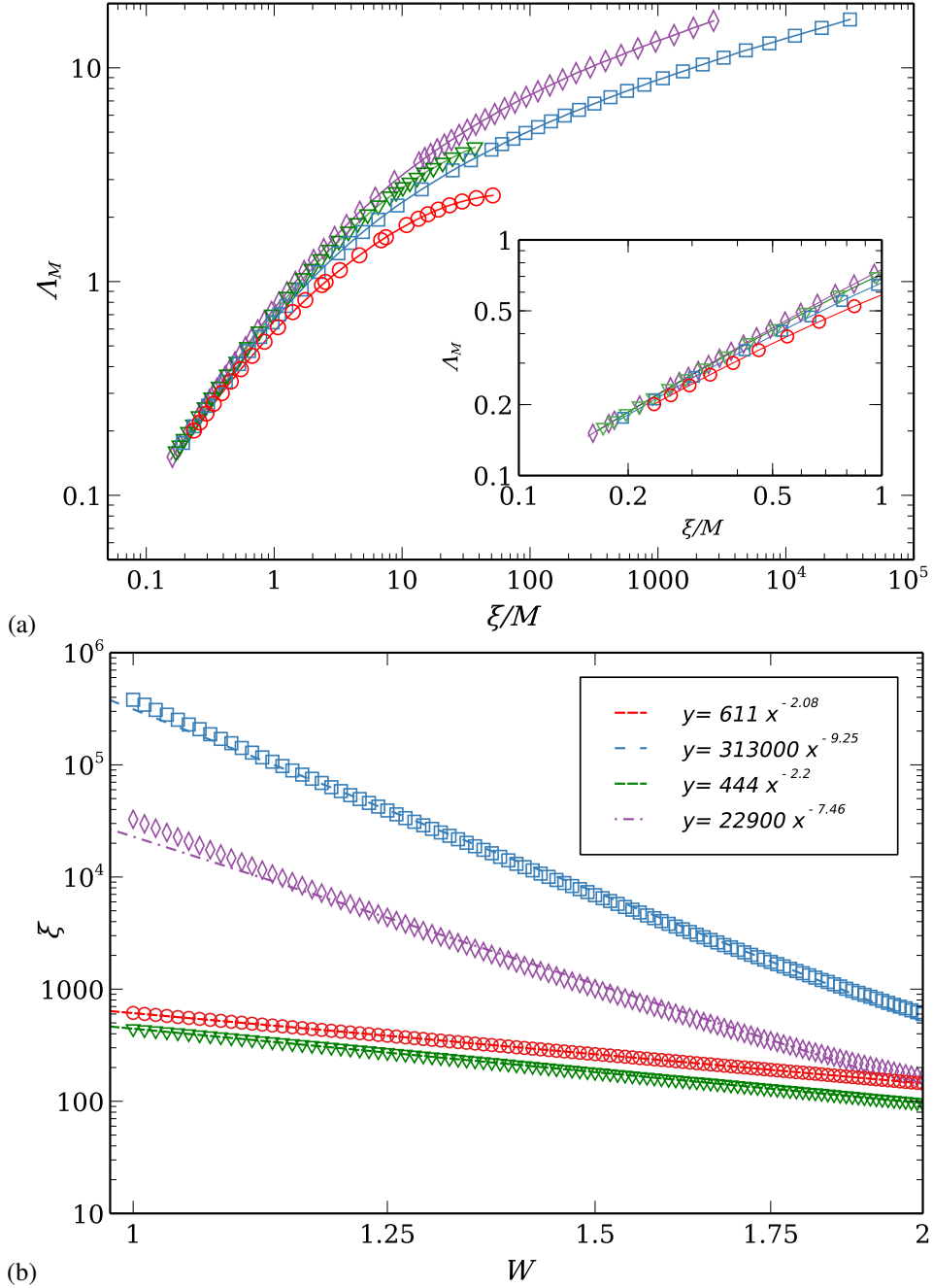


Figure 2: (a) Scaled localization length $\Lambda_M(0, W)$ versus ξ/M at energy $E = 0$ for $\mathcal{L}_2(1)$ (red \circ), $\mathcal{L}_2(2)$ (blue \square), $\mathcal{L}_2(3)$ (green ∇) and $\mathcal{L}_2(4)$ (purple \diamond). For clarity, lines show all data points while symbols denote only about 15% of all data. Inset: the detail of small reduced correlation length. (b) Scaling parameters $\xi(0, W)$ for the same Lieb lattices as in (a). The dashed lines represent the power law fit functions ax^b . Error bars are within symbol size in both panels.

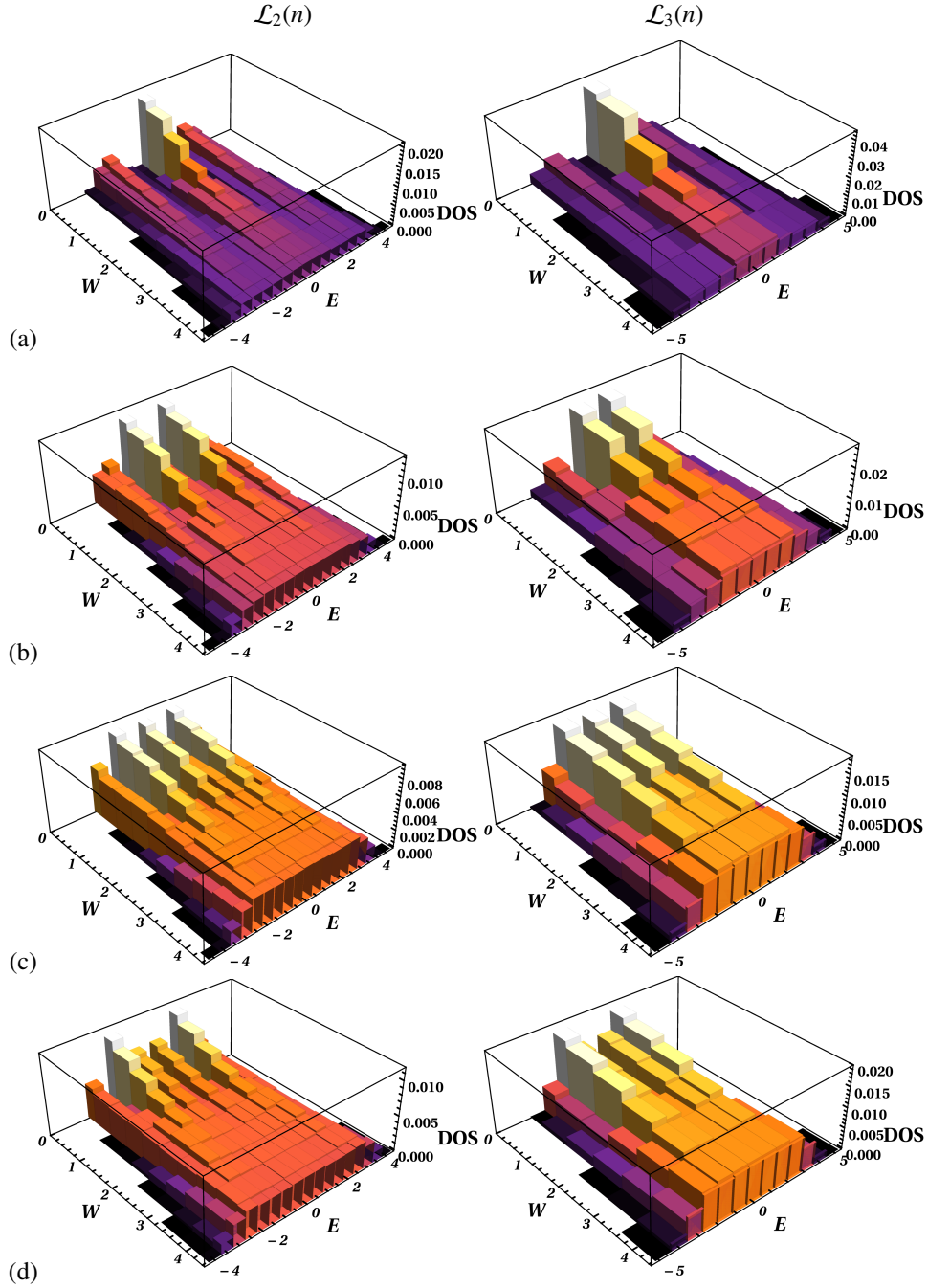


Figure 3: Normalized bar chart histograms of the (E, W) -dependence of the density of states (DOS) for (a) $\mathcal{L}_2(1)$ and $\mathcal{L}_3(1)$, (b) $\mathcal{L}_2(2)$ and $\mathcal{L}_3(2)$, (c) $\mathcal{L}_2(3)$ and $\mathcal{L}_3(3)$, and (d) $\mathcal{L}_2(4)$ and $\mathcal{L}_3(4)$. The colors denote different DOS values ranging from zero (deep purple) to maximal (white). Bin widths in (E, W) directions have been chosen for representational clarity.

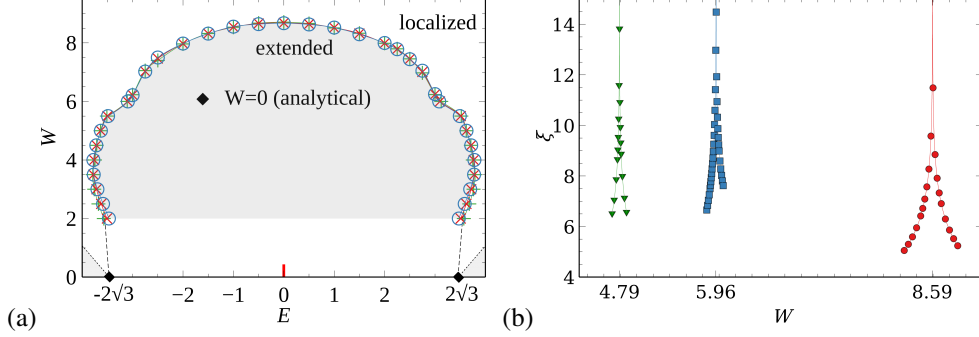


Figure 4: (a) Phase diagram for $\mathcal{L}_3(1)$ in case of periodic boundaries. The three solid and colored lines represent the approximate location of the phase boundary estimated from small M , i.e. the blue line/ \circ comes from widths $M = 4$ and $M = 6$, the red line/ \times from $M = 4$ and $M = 8$, and the green line/ $+$ from $M = 6$ and $M = 8$. The shaded area in the center contains extended states while states outside the phase boundary are localized. The dashed lines on both sides are guides-to-the-eye for the expected continuation of the phase boundary for $W < 2$. The red short vertical line at $E = 0$ represents the position of the doubly-degenerate flat band. The diamonds (\blacklozenge) denote the band edges for $W = 0$, i.e. $E_{\min} = -2\sqrt{3}$ and $E_{\max} = 2\sqrt{3}$. The dotted lines are the theoretical band edges $\pm(|E_{\min}| + W/2)$ and the forbidden areas below those band edges have been shaded. (b) Scaling parameters ξ versus disorder W for $\mathcal{L}_3(1)$ (red \circ), $\mathcal{L}_3(2)$ (blue \square) and $\mathcal{L}_3(3)$ (green ∇) at energy $E = 0$. The expansion parameters n_r, n_i, m_r and m_i are the same as the highlighted line in Table 1.

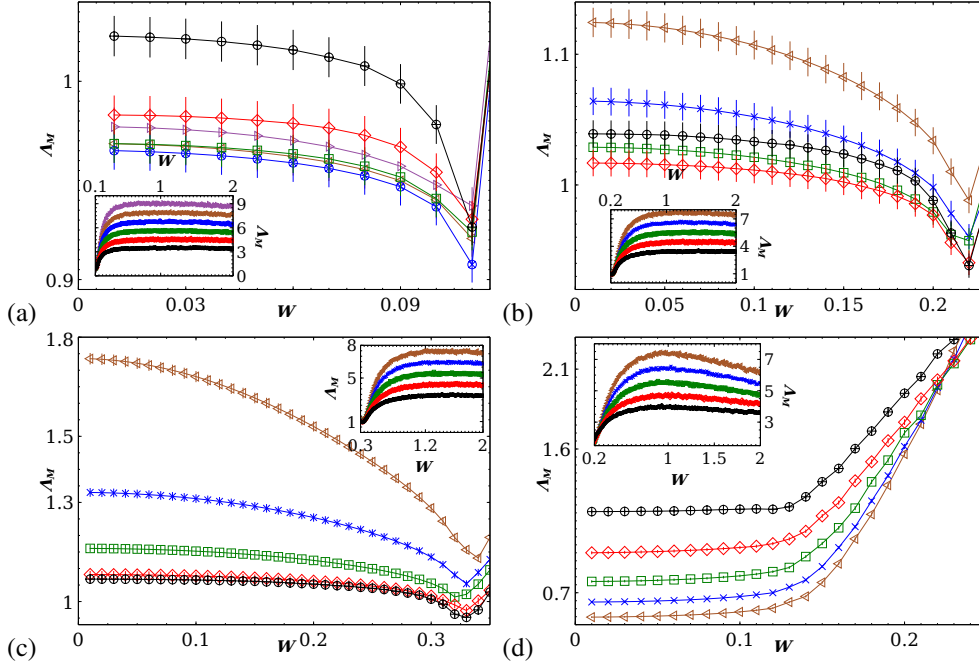


Figure 5: (a) Small W behaviour of Λ_M for $\mathcal{L}_3(1)$ with (a) energy $E = 0.05$, (b) $E = 0.1$, (c) $E = 0.15$, and (d) for $\mathcal{L}_3(2)$ at $E = 1.05$ with disorder down to 0.01 in steps of 0.01 and with error less than 1.0%. System sizes M are 4 (black \oplus), 6 (red \diamond), 8 (green \square), 10 (dark-blue \times), 12 (brown \triangleleft), 14 (purple \triangleright). Error bars are denoted with a solid line. Insets: increased disorder range up to $W = 2$ for the corresponding cases in the 4 main panels.